International Journal of Heat and Mass Transfer 52 (2009) 3225–3234

Contents lists available at ScienceDirect

International Journal of Heat and Mass Transfer

journal homepage: www.elsevier.com/locate/ijhmt

Validation of fully implicit method for simulation of flows with interfaces using primitive variables

Kausik Nandi, A.W. Date *

Mechanical Engineering Department, Indian Institute of Technology, Bombay, Mumbai 400076, India

ARTICLE INFO

Article history:
Received 10 June 2008
Received in revised form 26 October 2008
Accepted 5 January 2009
Available online 25 March 2009

Keywords:
Single fluid formalism
Surface tension force
Dam break
Splashing
Sloshing
Bubble burst and merger
Interface instability

ABSTRACT

This paper describes applications of the fully implicit procedure for computing flow of two immiscible fluids. Six problems in two and three dimensions are solved to highlight effects of grid size, pressure smoothing, TVD convection scheme and geometric and fluid dynamic evaluations of surface tension force. Free surface and cavity flows are considered in which effect of sloshing, interface merger and splitting as well as splashing are included. Wherever possible, present solutions are compared with results of previous experiments and/or numerical computations. Computational details such as grid size, time step, under-relaxation factors, mass/volume conservation are reported.

© 2009 Published by Elsevier Ltd.

1. Introduction

The fully implicit numerical procedure for prediction of flows with interfaces has been described in Ref. [1]. This procedure has employed novel means to avoid problems of zig-zag pressure predictions on collocated grids, loss/gain of mass/volume encountered in some of the previous methods and, interface smearing associated with simple upwind difference scheme in the advection equation. Further, evaluation of the surface tension force from mean pressure difference across the interface has been newly introduced. The purpose of the present paper is to demonstrate validity of these theoretically derived procedures against following six problems:

(1) Rayleigh–Taylor instability (2D).
(2) Collapse of a water column (2D).
(3) Sloshing in a tank (2D).
(4) Splashing of a water drop on a water surface (2D).
(5) Bursting of a rising bubble through liquid surface (3D).
(6) Merger of two rising bubbles in a tank of liquid (3D).

Experimental data and/or numerical computations for all problems are available in the literature. Surface tension force is evaluated in 3D problems but ignored in 2D problems. Complete computational details are given in the text of this paper. All computations are performed on a Xeon (3.2 GHz) dual processor work station. 2D problems are solved in single precision and 3D problems are solved in double precision by adapting Computer Code given in Date [13]. All figures in this paper are plotted using TECPLOT.

2. Results and discussion

In all problems presented and discussed suffix a refers to heavier fluid and suffix b to the lighter one. Also, pressure and velocity are set to zero by way of initial conditions in all problems.

2.1. Rayleigh–Taylor instability

We consider the problem as specified by Rudman [2] (see Fig. 1a). Heavier fluid with $\rho_a = 1.2$ at the top is separated from the lighter fluid $\rho_b = 1.0$ in a two-dimensional cavity $2L \times 3L$. The interface is located at $x_2 = 2L$ from the bottom. The Froude number $Fr = U_{ref}/(gL)^{0.5} = 0.5$. In order that the Reynolds number $Re = (U_{ref}\,\rho L/\mu)_{a,b} = 500$ in both fluids is the same, the fluid viscosities are taken as $\mu_a = 0.0037582$ and $\mu_b = 0.00313182$. Further, $\sigma = 0$.

Exploiting symmetry, the domain of computation is taken as shown in Fig. 1b with symmetry plane at $x_1 = 0$. At $t = 0$, the interface is perturbed according to $(x_2/L) = 2 + 0.02\cos(2\pi x_1/L)$. The consequence of this physical displacement of the interface is reflected in the initial F distribution in control volumes on either side of the interface. Taking $g = 9.81$ and $L = 1$, the computations

* Corresponding author. Tel.: +91 022 2576 7517; fax: +91 022 2572 6875.
E-mail address: awdate@me.iitb.ac.in (A.W. Date).

0017-9310/$ - see front matter © 2009 Published by Elsevier Ltd.
doi:10.1016/j.ijheatmasstransfer.2009.01.035

Nomenclature

D	diameter
F	volume fraction
Fr	Froude number
F_{st}	surface tension force
g	gravity acceleration
L and H	domain length and height
Re	Reynolds number
t	time
u_i	velocity in $x_i, i = 1,2,3$ direction
V	volume
$\vec{V}$	total velocity vector
We	Weber Number

Greek symbols

μ	dynamic viscosity
ρ	density
σ	surface tension coefficient

Suffixes

a	refers to heavier fluid
b	refers to lighter fluid
n	normal to the interface
x_i	refers to $x_i, i = 1,2,3$ directions

are performed with fixed time step $\Delta\tau = 0.001$ where $\tau = 0.5 \times t \times (g/L)^{0.5}$ and with 20×60, 40×120 and 80×240 uniform control volumes in x_1 and x_2 directions, respectively. At the first time step, iterations in excess of 500 were required to achieve convergence. After 20 time steps, the number of iterations required was less than 12 per time step. The maximum error in volume balance was found to be 1.03% on the coarsest grid but was reduced to 0.46% on the finest grid.[1] Computed contours of $F = 0.5$ are plotted in Fig. 2 for $\tau = 4$, 6 and 8 on three grids. It is seen that as the grid is refined, finer structures in the flow are increasingly resolved. The present results bear similarity with those computed by Rudman [2] using FCT-VOF discretization of the advection equation.

Fig. 3 shows comparison of F-distributions ($0.025 < F < 0.975$) obtained by TVD [15,16] and UDS schemes on 80×240 grid. The figure confirms that TVD predictions show much less smearing than the UDS scheme. None-the-less, sharpness of interface predictions is still less than satisfactory when the interface is inclined with respect to the grid lines.[2] These remarks also apply to several other TVD schemes (see [7,17–21]).

Finally, Fig. 4 shows pressure contours and velocity vectors obtained using TVD scheme. The velocity vectors confirm that the distribution of volume fraction F(see Fig. 3) is governed by convection. At small time, a single (double in the full cavity) vortex is seen in the heavier fluid which then breaks into two re-circulating regions at $\tau = 6$. At $\tau = 8$, the vortex near the symmetry axis elongates in the downward direction while the vortex in the top-right corner becomes larger. Likewise, the pressure contours begin to deviate from pure hydrostatic variations at small times as the heavier fluid descends near the axis of symmetry. Closed loop contours are seen at larger times surrounding vortex centers.

2.2. Collapse of a water column

Fig. 5 shows the configuration of the problem. The computational domain is 4 m × 2.2 m. Initially, water (fluid a) column $H = 2$ m high and $L = 1$ m wide is kept at rest by means of a dam. Fluid b is air. At $t = 0$, the dam breaks. It is of interest to predict variations of vertical height $Y(t)$ at $x_1 = 0$ and horizontal spread $X(t)$ at $x_2 = 0$ as functions of time following the break. Surface tension effects are not considered.

Computations are performed with 40×22 uniform control volumes (same as that used by Jun and Spalding [3]) in x_1 and x_2 directions, respectively. Taking $g = 9.81$ and $L = 1$, fixed time step $\Delta\tau = 0.001$ is used where $\tau = t \times (2 \times g/L)^{0.5}$. The density and viscosity of the two fluids are taken as $\rho_a = 998.1$, $\rho_b = 1.205$, $\mu_a = 0.00101$ and $\mu_b = 1.81 \times 10^{-5}$. The ratios of properties of fluid a to fluid b are thus formidably high. In order to obtain good convergence, it was found necessary to under-relax pressure correction equation in the initial stages of flow development. No-slip condition for velocities and zero-flux condition for *F-equation* were used as boundary conditions at all boundaries. Computations are carried out till $\tau = 3$. At this time, the maximum error in volume balance was found to be 0.432%.

The time variations of X and Y are compared in Fig. 6 with experimental data presented in Tables 2 and 6 of the paper by of Martin and Moyce [5]. The comparison is reasonable not-withstanding the experimental difficulties mentioned by Martin and Moyce [5]. Fig. 7 shows the $F = 0.5$ contours at four different times. These contours mimic those presented in Ref. [3] using the conserved-scalar equation and explicit van Leer scheme [4].

2.3. Sloshing in a tank

Fig. 8 shows the problem specification. The tank is moved with a horizontal displacement

$$x_1(t) = A\{\sin(2\pi f_1 t) - \sin(2\pi f_2 t)\}$$

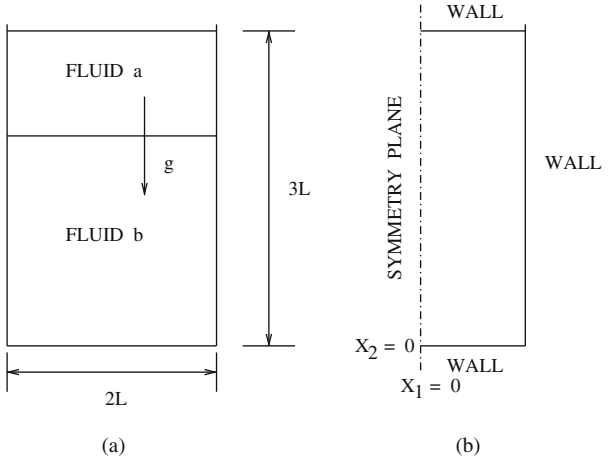

Fig. 1. Rayleigh–Taylor instability: (a) problem specification (b) domain of computation.

[1] The present calculations are performed using single precision. They demonstrate higher volume errors than when double precision is used as in 3D computations presented later in this paper.

[2] Many authors test the efficacy of a TVD or any other higher order convection scheme by considering a variety of problems in which velocity distributions are prescribed. Then, only ρ_m (or, F or level set) equation is relevant [1]. Also, the predicted F-distributions are not compared with any experimental data obtained with real fluids. As such, we regard such test cases as purely mathematical constructs because pressure and viscosity are not permitted to influence the interface evolution. It is for this reason, we believe, that Rudman [2] has, in effect, remarked that *accurate representations of convective fluxes in an isolated F-equation does not guarantee accurate predictions when flow velocities are calculated from N–S equations.*

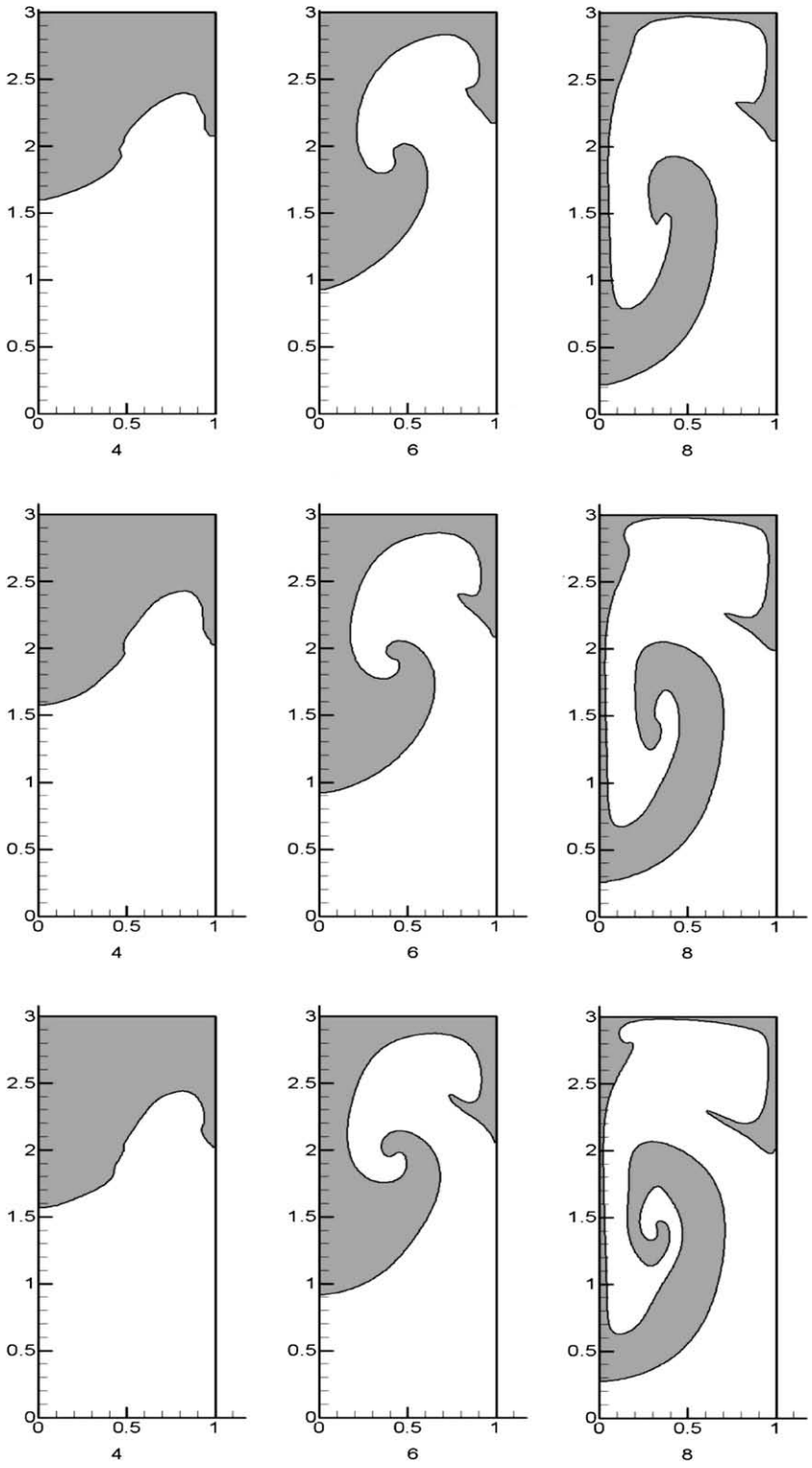

Fig. 2. Rayleigh–Taylor instability – 20×60 (top), 40×120 (middle), 80×240 (bottom) – dark portions represent heavier fluid *a*.

where $A = 7.5 \times 10^{-3}$, $f_1 = 1.598$ Hz and $f_2 = 1.307$ Hz. Computations are performed with 60×60 cells and time step $\Delta t = 0.001$ s. Fluid properties are same as in the previous problem and $\sigma = 0$. On all boundaries, $u_1(t) = dx_1/dt, u_2 = 0$ was specified at each time step. *F*-Equation was solved with zero-flux boundary condition. Nearly 500 iterations per step are required to obtain convergence. The pressure correction equation was under-relaxed in the first 100 time steps to procure convergence. At $t = 2.004$ s, the volume error was 0.45%. In Fig. 9, the predicted interface profiles (lines) are compared with experimental data (dots) as read from paper by Andrillon and Alessandrini [6]. Again, the agreement between experimental data and numerical results is reasonable. Fig. 10 shows dimensionless pressure $p^* = (p - p_{min})/(p_{max} - p_{min})$ contours and velocity vectors at different times. The velocity in the air greatly exceeds that in the water. The fluid re-circulations due to interface movement accord with the expectation and the pressure contours are indeed smooth (see Date [14]). The pressure distributions enable evaluation of forces acting on tank walls.

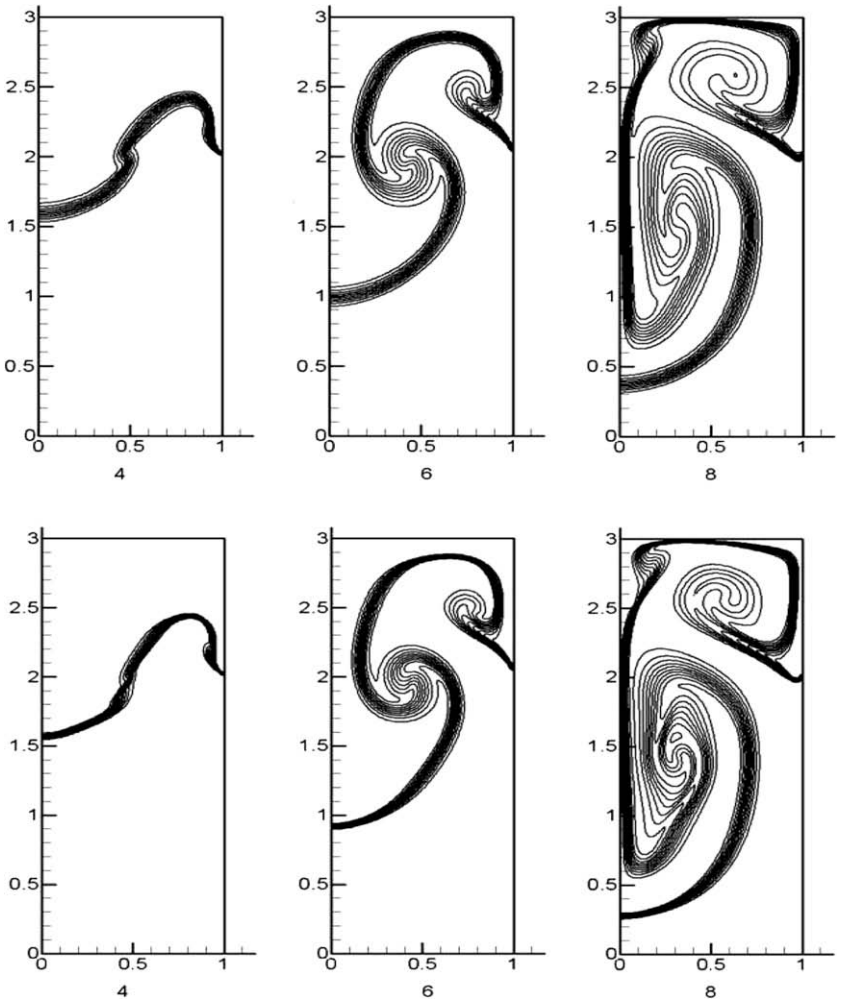

Fig. 3. Comparison of UDS (top) and TVD (bottom) predictions.

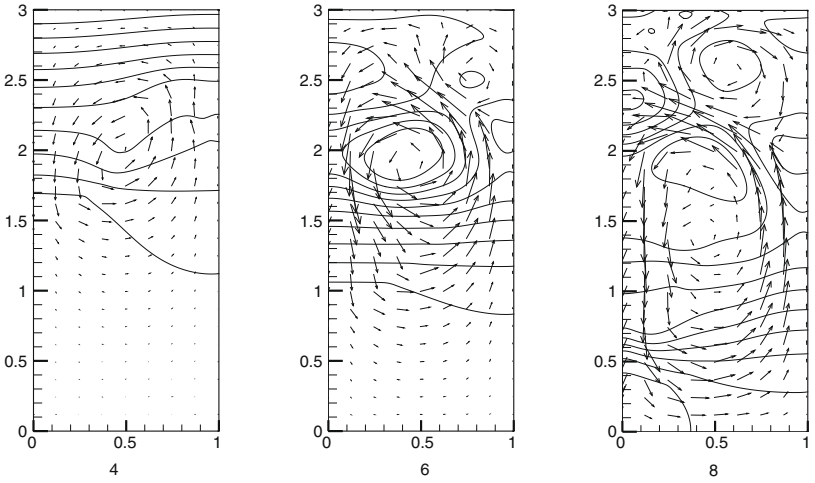

Fig. 4. Rayleigh–Taylor instability (80×240) – pressure contours and velocity vectors (scale: 1 cm = 1 m/s) with TVD scheme.

2.4. Splashing of a water drop on a water surface

Consider a two-dimensional rectangular enclosure of 7 mm× 14 mm dimensions. The enclosure is filled with water to a height of 8.75 mm. Initially a cylindrical water drop of radius $r_d = 1.4$ mm is placed above the water surface in air at the center plane $x_1 = 3.5$ mm and height $x_2 = 10.55$ mm. For $t > 0$, the drop falls under the action of gravity ($g = 9.81$ m/s^2) and splashes on the water surface creating ripples and merges with the body of water. The fluid properties are same as those in the dam-break problem.

Computations are performed with 64×128 grid without exploiting symmetry. Fifty iterations per time step (10^{-5} s) are re-

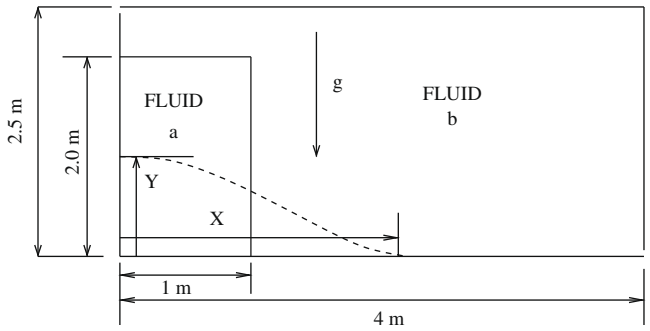

Fig. 5. Collapse of a water column – domain of computation.

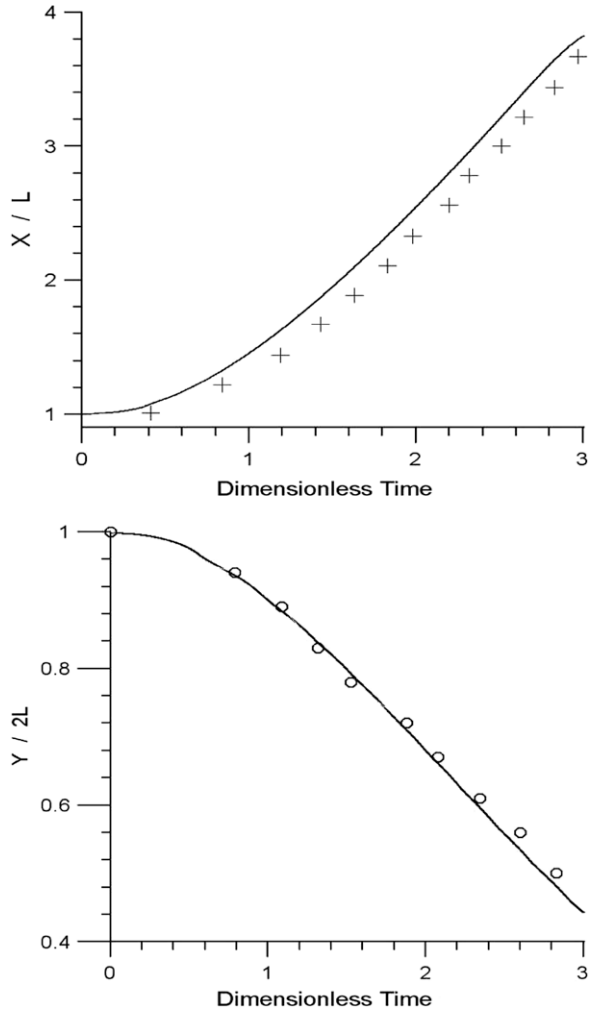

Fig. 6. Variation of horizontal spread X and vertical height Y with time – solid line (predictions), open circles (experimental data [5]).

quired with p' under-relaxed for obtaining convergence. Computations are continued up to $t = 0.025$ s and the interface profiles are shown in Fig. 11. This problem has also been computed by Puckett et al. [8] using VOF method with interface reconstruction at every time step although the exact dimensions of the cavity are not mentioned in their paper. The present results are qualitatively in accord with their predictions with maximum volume error 0.002% although the air entrapment in water following the splash observed by them is not obtained by us most probably due to coarseness of the grid.

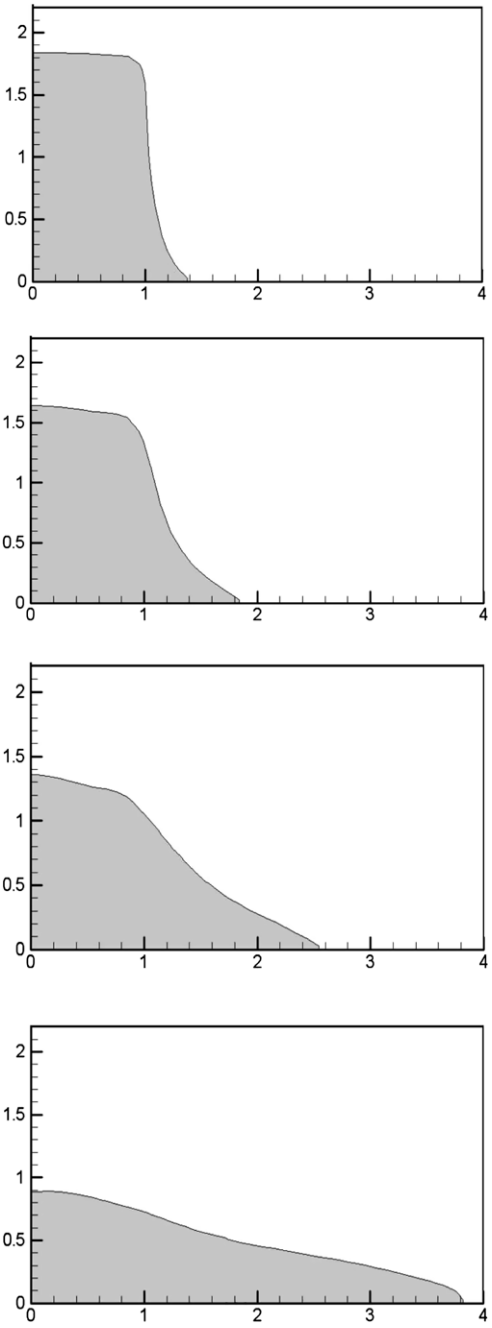

Fig. 7. Interface locations at $\tau = 0.9,\ 1.4,\ 2.0$ and 3.0. Collapse of a water column – dark portions represent water.

Fig. 12 shows the development of pressure and velocity in the enclosure. It is interesting to note that as soon as the drop begins to fall, upward flow is generated in air near the vertical walls and which then recirculates near the water surface causing shear. This induces motion in the water even when the drop is not in contact with water. These motions cause development of pressure variations that deviate from pure hydrostatic pressure variation.

2.5. Bursting of a bubble

Fig. 13 shows a three-dimensional box of dimensions $6 \times 6 \times 12$ U which is filled with liquid up to 4 U height. A bubble

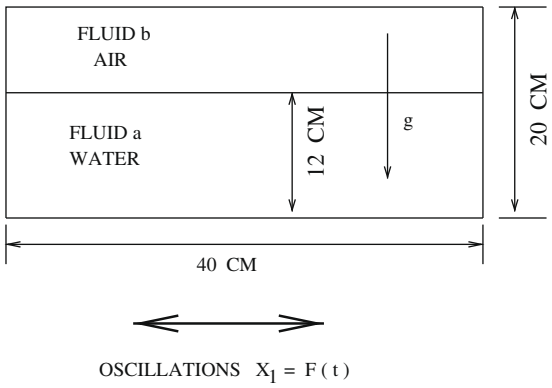

Fig. 8. Sloshing in a tank.

of diameter $D = 2$ U is introduced with its center at (3,3,2.8) at $t = 0$. Due to buoyancy, the bubble rises and bursts through the free liquid surface entraining with it some liquid. The equations are solved with periodic boundary conditions at (x and y) = 0 and 6 U whereas no-slip conditions are used at $z = 0$ and 12 U.

This problem has been solved by Takahira et al. [9] using the level-set method using $60 \times 60 \times 120$ grid and the surface tension force is evaluated from geometric considerations (which requires value of σ). Here, in order to save computer time, the same problem is solved on coarser grid of dimensions $30 \times 30 \times 60$. Maximum of 50 iterations per time step ($\Delta\tau = 0.001$) are required to procure convergence. The reference velocity U_{ref}, properties ρ_a, μ_a and surface tension coefficient σ are chosen such that

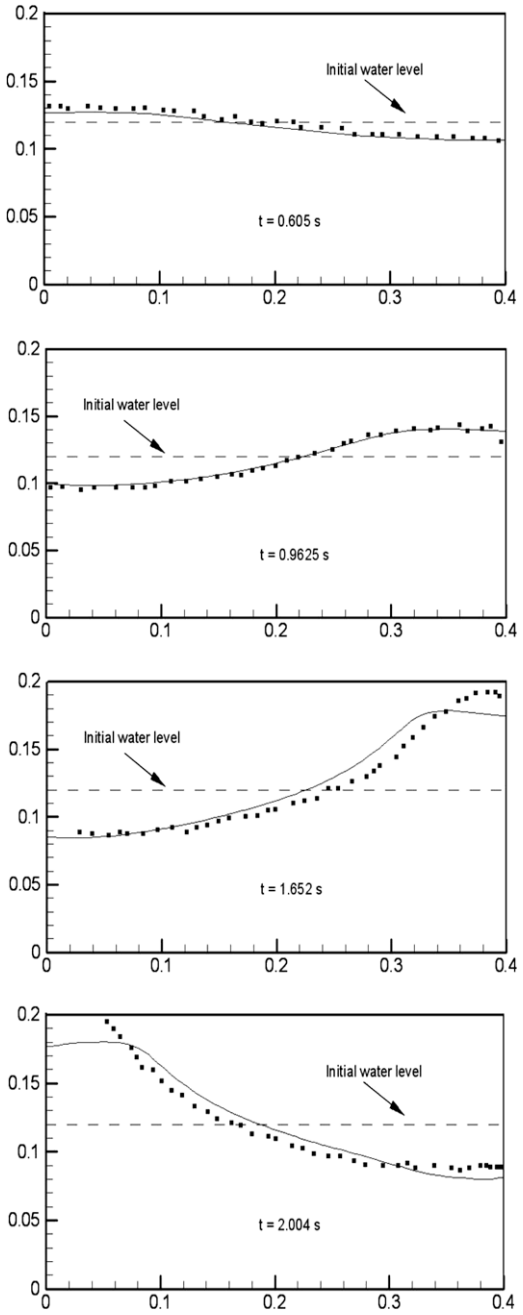

Fig. 9. Interface locations – sloshing in a tank.

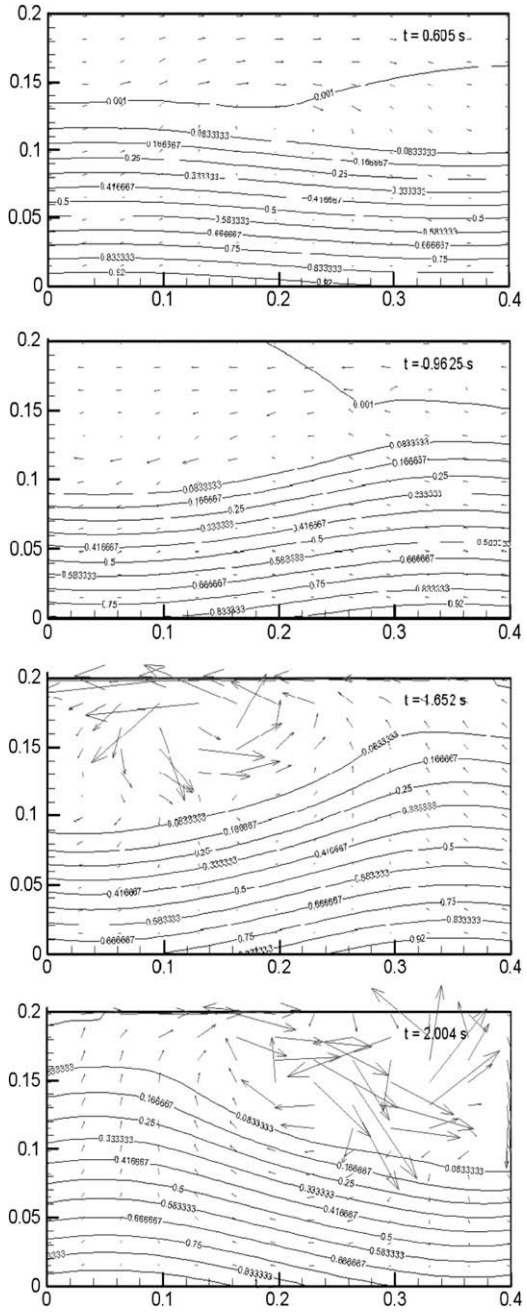

Fig. 10. Pressure contours and velocity vectors (arrow size: 1 cm = 0.13 m/s) – sloshing in a tank.

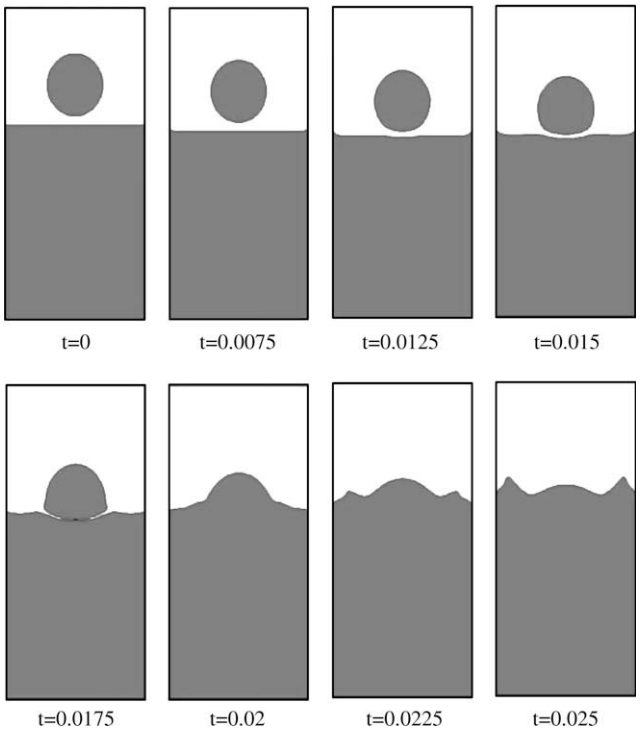

Fig. 11. Splashing of a water drop on a surface – dark portions represent water.

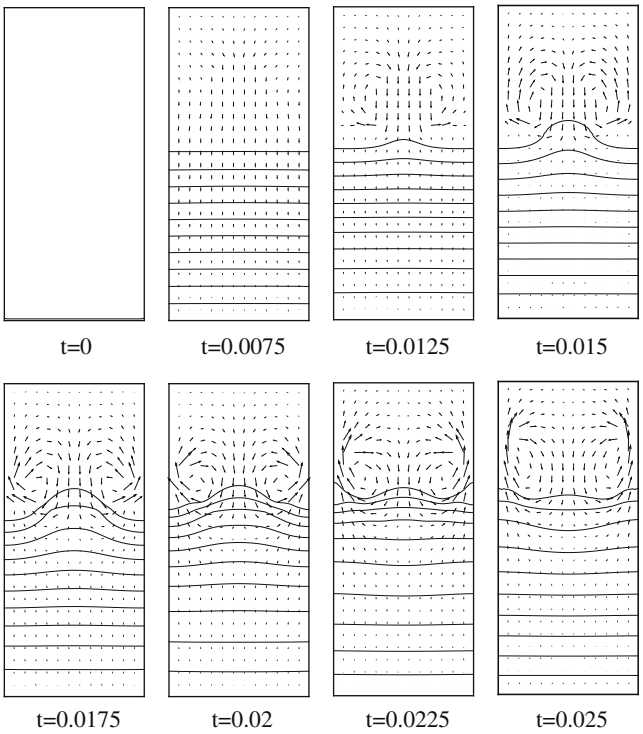

Fig. 12. Splashing of a water drop on a surface – pressure contours and velocity vectors (scale: 1 cm = 2 m/s).

$$Re = \frac{\rho_a U_{ref} D}{\mu_a} = 474, \quad We = \frac{\rho_a U_{ref}^2 D}{\sigma} = 1.0$$

$$Fr = \frac{U_{ref}^2}{gD} = 0.64, \quad \frac{\rho_b}{\rho_a} = 0.001, \frac{\mu_b}{\mu_a} = 0.01$$

$$\tau = t \times \frac{U_{ref}}{D}$$

Here, computations are performed with geometric (using value of σ) as well as fluid dynamic evaluations (without using σ) of surface tension force [1]. In both cases, computations are extended to dimensionless time $\tau = 1.68$.

Fig. 14 shows the $F = 0.5$ distributions at time intervals chosen in Ref. [9]. It is seen that predictions with both types of evaluations are nearly identical. The predictions also accord with those obtained by Takahira et al. [9] although the burst heights at large times are somewhat smaller due to coarseness of the grid used here. None-the-less the formation of ripples on the liquid surface are clearly seen at $\tau = 0.4$ and 0.72. Likewise, at $\tau = 1.4$ and 1.68, formation of a *neck* in the entrained liquid suggests that a detached liquid drop is about to form. These fine features would become clearer if computations are carried out on a very fine grid.

Since predictions with both types of evaluations are nearly identical, we have computed this problem *without surface tension force* ($F_{st} = 0$). Fig. 15 shows the computed results. It is seen that now the burst heights are greater indicating that the absence of surface tension force fails to minimise the interface-surface during bursting, as expected.

Finally, Fig. 16 shows the time variation of volume error given by

$$\text{Error} = \frac{\sum F_{i,j} \Delta V_{i,j}}{\sum F_{i,j}^0 \Delta V_{i,j}}$$

where F^0 is the initial F-distribution at $t = 0$. It is seen that the maximum error with fluid dynamic evaluation of F_{st} is 0.078%. The same was found to be 0.093% (not shown here) with geometric evaluation. These errors are much smaller than the one reported by Takahira et al. [9] on a finer grid ($60 \times 60 \times 120$). In addition, Takahira et al. also had to employ an *ad hoc* correction factor 1.08 during re-initialisation in their level-set method to obtain reasonably small volume error.

2.6. Merger of two rising bubbles

Following Takahira et al. [9], in this problem we consider a computational box similar to the one shown in Fig. 13. The size of the box is $4 \times 4 \times 12$ U spanning $-2 < x < 2, -2 < y < 2, -6 < z < 6$. The box is filled with liquid and initially (at t = 0) two spherical bubbles (diameter D = 2) are asymmetrically placed at $(0.25, 0, -4.5)$ and $(-0.25, 0, -2.3)$. Due to buoyancy, the two bubbles rise and due to the associated fluid motion, the bubbles merge into one bubble after a certain time. Both bubbles deform during this process developing non-spherical shapes. It is of interest to study the topography of the bubbles and the merger time. We follow specifications of Takahira et al. [9]

$$Re = \frac{\rho_a U_{ref} D}{\mu_a} = 50, \quad We = \frac{\rho_a U_{ref}^2 D}{\sigma} = 1.5$$

$$Fr = \frac{U_{ref}^2}{gD} = 1.0, \quad \frac{\rho_b}{\rho_a} = 0.001, \quad \frac{\mu_b}{\mu_a} = 0.01816$$

No-slip condition is used on all walls of the box and zero-gradient condition is used for ρ_m (or F). The grid size is $30 \times 30 \times 90$ whereas Takahira et al. have used $50 \times 50 \times 150$. In this problem we have used only *fluid dynamic evaluation of the surface tension force*. As such, the value of σ (or We) is not required. Equations are solved with $\Delta\tau = 0.001$ s and 50 iterations per times step are executed. To obtain convergence, pressure correction equation had to be under-relaxed with $\alpha_{p'} = 0.001$. Computations are continued till dimensionless time $\tau = 4$ when the maximum volume error was found to be 0.054%. Takahira et al. [9], in their level-set method found the error to be 2% which was reduced by an *ad hoc* tuning factor 1.05 in volume conservation during the re-ini-

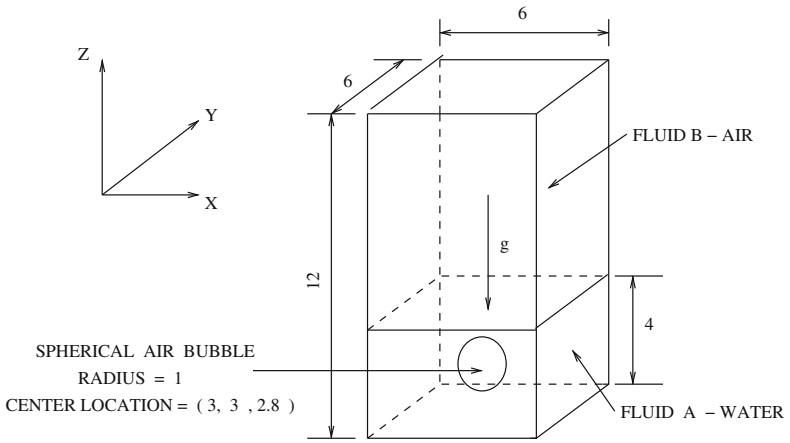

Fig. 13. Bursting of a bubble.

tialisation step in their level-set method. The present predictions show (see Fig. 17) following features:

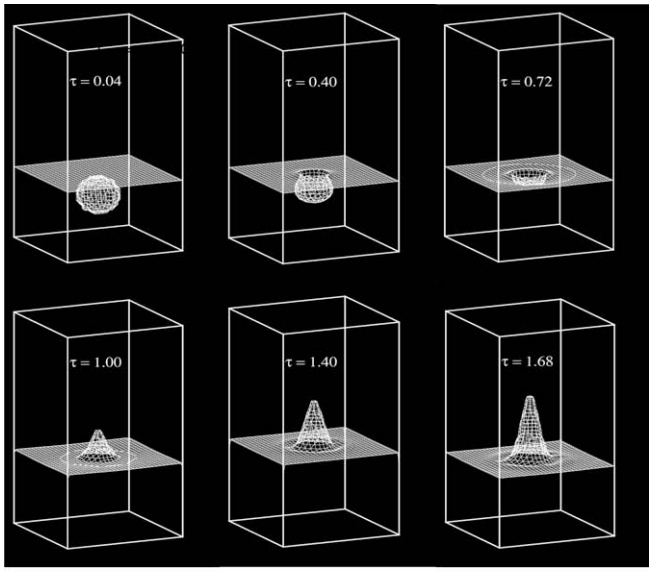

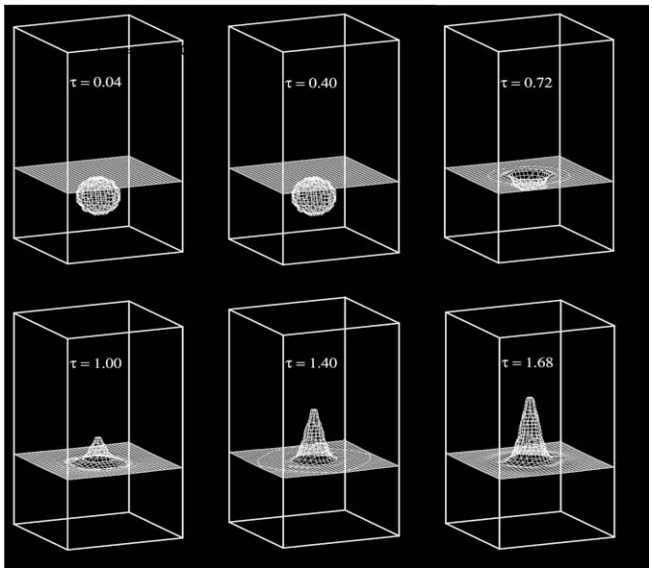

Fig. 14. Bubble burst – (top) geometric evaluation of f_{st}, (bottom) fluid dynamic evaluation of F_{st}.

(1) Both bubbles begin to rise simultaneously but the bottom bubble moves up somewhat faster than the upper bubble. Merging is initiated at $\tau = 1$. In the level-set predictions of Takahira et al. [9], merger is initiated at $\tau \simeq 5.6$.

(2) After the commencement of merging process, the top bubble develops a spherical (more ellipsoidal) cap and its underside folds upwards providing *suction* to deform the lower bubble into a pointed tail-like structure. The spherical cap structure with upward folding of the underside has been experimentally observed for a single bubble rise by Hnat and Buckmaster [22]. But, no such sphericity is found in predictions of [9]. In fact, their upper bubble is much more *squashed* ellipsoid than spherical nor does it show any significant upward folding of the underside.

(3) The tail-like structure of the lower bubble is seen up to $\tau = 4$ while the upper bubble maintains sphericity though somewhat skewed. This type of behaviour has been obtained by Shin and Juric [23] who used projection method with interface reconstruction and evaluated curvature by geometric method to compute rise of two asymmetrically placed bubbles in a $1 \times 1 \times 2$ box. The parameters in their computations however were different. In terms of the present definitions, they computed following cases[3]

$$Re = 18.8 \quad \text{and} \quad 72.08, \quad We = 50 \quad \text{and} \quad 300$$
$$Fr = 1.0 \ \frac{\rho_b}{\rho_a} = 0.05 \ \frac{\mu_b}{\mu_a} = 0.04 \text{ in both cases}$$

Their predictions of the bubble development in the two cases show far more pronounced effect of *Re* than We. Note that their *Re* values are comparable to that in the present computations whereas their *We* values are much higher (very small σ). Similarly, their density ratio is 50 times greater whereas the viscosity ratio is greater by a factor of about 2 compared to the values used in the present investigation. Not-withstanding these differences, the bubble structures in the present predictions are similar to those computed by them.[4]

(4) The comparisons with predictions of Shin and Juric [23] mentioned above again suggest that Weber number is not

[3] Shin and Juric [23] specified Etovos number (Eo) and Morton number (M) as

$$Eo = \frac{We}{Fr} = 50 \quad \text{and} \quad 300, \quad M = \frac{We^3}{Re^4 \times Fr} = 1$$

[4] Unfortunately, Shin and Juric [23] do not mention either dimensional or non-dimensional times in their figures to comment further.

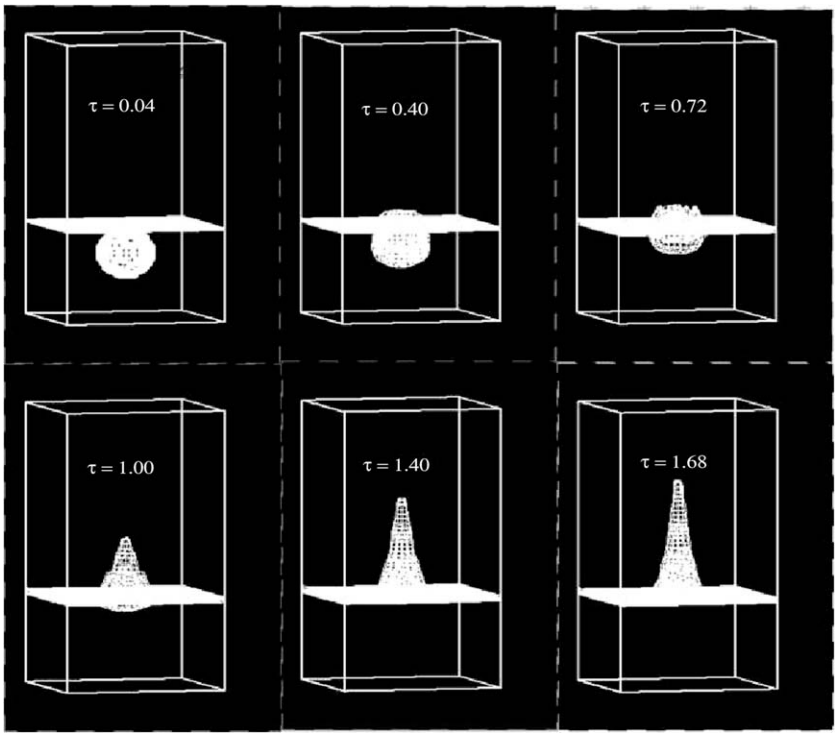

Fig. 15. Bubble burst – predictions without surface tension force ($F_{st} = 0$).

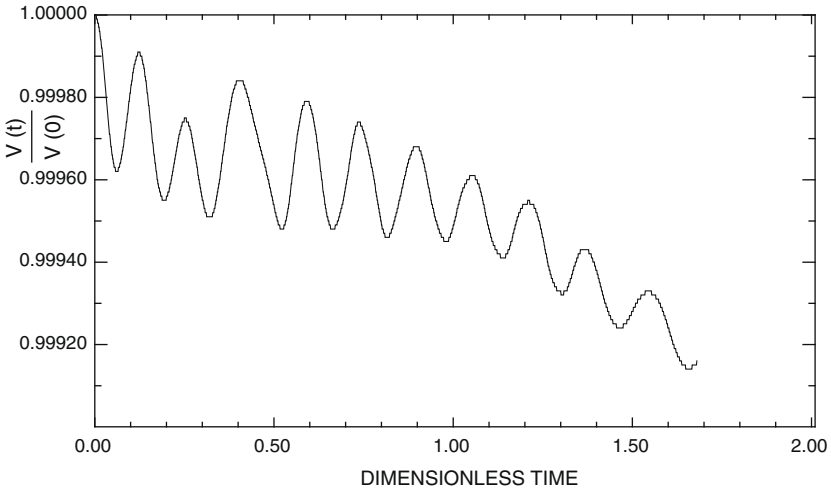

Fig. 16. Volume error – fluid dynamic evaluation of F_{st}.

an influencing parameter in bubble merger. This result coupled with the comparisons with the experimental observations of [22] confirm our view that Weber number is not an independent parameter as theoretically shown in Ref. [1].

3. Conclusions

(1) In this paper, six unsteady problems involving flow of immiscible incompressible fluids are solved within the single fluid formalism. The governing equations are solved using fully implicit SIMPLE algorithm on collocated grid as described in Ref. [1].

(2) The results from four 2D problems without surface tension have agreed with previous numerical results and experimental data from the literature. In each problem, additional features such as smoothness of pressure contours, velocity vectors, effect of grid size, reduced interface smearing due to use of TVD scheme, extent of volume/mass conservation, effect of external forces as in sloshing of a tank problem, interface merger as in splashing of a drop problem, etc. have been highlighted.

(3) The results from two 3D problems involving single bubble burst and merger of two asymmetrically placed bubbles have confirmed that fluid dynamic evaluations of surface tension force predict development of bubble shapes that accord with experiment as well as previous computations

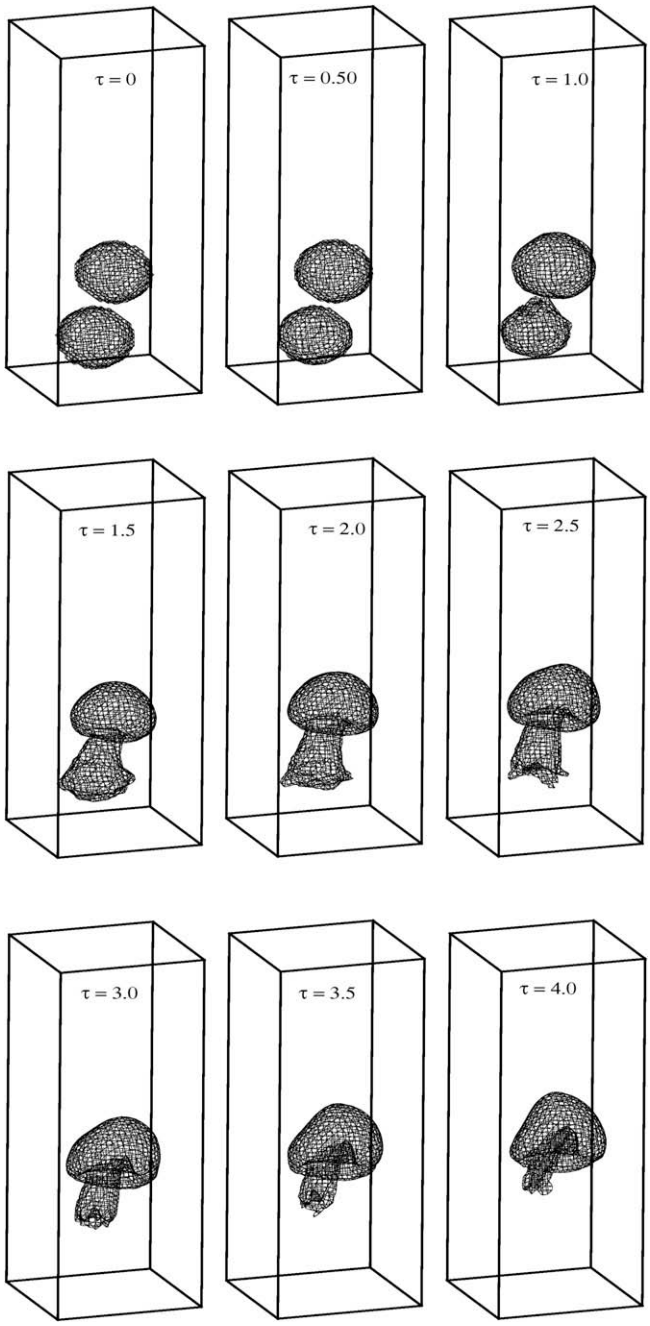

Fig. 17. Merger of two rising bubbles in liquid.

employing interface reconstruction and evaluation of surface tension force based on geometric evaluation of interface curvature. In both problems, excellent volume/mass conservation has been obtained. This finding represents a major departure from all previous publications (see [9–12] for example) known to us.

(4) The applications presented in the paper have shown that the formulation developed in the companion paper [1] is robust and capable of predicting all features of the flow that have been previously predicted using alternative methods for solving the governing equations. Of course, to reduce computer times in 3D computations, use of solution dependent adaptive grids [24] is desirable.

Acknowledgement

The present research is funded by Board of Research in Nuclear Sciences under Project No. 2005/36/47/BRNS.

References

[1] K. Nandi, A.W. Date, Formulation of Fully Implicit Method for Simulation of Flows with Interfaces Using Primitive Variables, Companion Paper, this volume.
[2] M. Rudman, Volume-tracking methods for interfacial flow calculations, Int. J. Numer. Methods Fluids 24 (1997) 671–691.
[3] L. Jun, D.B. Spalding, Numerical simulation of flows with moving interfaces, Physico-Chem. Hydrodyn. 10 (1988) 625–637.
[4] B. van Leer, Towards the ultimate conservative difference scheme IV, a new approach to numerical convection, J. Comput. Phys. 23 (1977) 276.
[5] J.C. Martin, W.J. Moyce, An experimental study of collapse of liquid columns on a rigid horizontal plane, Philos. Trans. R. Soc. Lond. A: Math. Phys. Eng. Sci. 244 (1952) 312–324.
[6] Y. Andrillon, B. Alessandrini, A 2D + T VOF fully coupled formulation for the calculation of breaking free-surface flow, J. Marine Sci. Technol. 8 (2004) 159–168.
[7] O. Ubbink, R.I. Issa, A method for capturing sharp fluid interfaces on arbitrary meshes, J. Comput. Phys. 153 (1999) 26–50.
[8] E.G. Puckett, A.S. Almgren, J.B. Bell, D.L. Marcus, W.J. Rider, A high order projection method for tracking fluid interfaces in variable density incompressible flows, J. Comput. Phys. 130 (1997) 269–282.
[9] H. Takahira, T. Horiuchi, S. Banerjee, An improved three dimensional level set method for gas–liquid two-phase flows, Trans. ASME J. Fluids Eng. 126 (2004) 578–585.
[10] A. Salih, S. Ghosh Moulic, Simulation of Rayleigh–Taylor instability using level-set method, Paper No. 1303, in: 33rd National and 3rd International Conference on Fluid Mechanics and Fluid Power, IIT Bombay, India, 2006.
[11] B.J. Daly, Numerical study of the effect of surface tension on interface instability, Phys. Fluids 17 (7) (1969) 1340–1354.
[12] D. Gerlach, G. Tomar, G. Biswas, F. Durst, Comparison of volume-of-fluid methods for surface tension dominant two phase flows, Int. J. Heat Mass Transfer 49 (2005) 740–754.
[13] A.W. Date, Introduction to Computational Fluid Dynamics, Cambridge University Press, New York, 2005.
[14] A.W. Date, Fluid dynamic view of pressure checker-boarding problem and smoothing pressure correction on meshes with collocated variables, Int. J. Heat Mass Transfer 48 (2004) 4885–4898.
[15] A.W. Date, Solution of Navier Stokes equations on non-staggered grid at all speeds, Numer. Heat Transfer B 33 (1998) 451–467.
[16] C.H. Lin, C. Lin, A simple high-order bounded convection scheme to model discontinuities, AIAA J. 35 (1997) 563–565.
[17] A. Harten, S. Osher, Uniformly high-order accurate non-oscillatory schemes, SIAM J. Numer. Anal. 24 (2) (1987) 279–309.
[18] J.J. Wei, B. Yu, W.Q. Tao, Y. Kawaguchi, H.S. Wang, A new high order accurate and bounded scheme for incompressible flow, Numer. Heat Transfer B 43 (2003) 19–41.
[19] P.H. Gaskell, A.K.C. Lau, Curvature-compensated convective transport: SMART, a new boundedness-preserving transport algorithm, Int. J. Numer. Methods Fluids 8 (1988) 617–641.
[20] J. Zhu, A low diffusive and oscillation-free convection scheme, Commun. Appl. Numer. Methods 7 (1991) 225–232.
[21] S. Vincent, J. Caltagirone, Efficient solving method for unsteady incompressible interfacial flow problems, Int. J. Numer. Methods Fluids 30 (1999) 795–811.
[22] J.G. Hnat, J.D. Buckmaster, Spherical cap bubbles and skirt formation, Phys. Fluids 19 (1976) 182–194.
[23] S. Shin, D. Juric, Modeling three-dimensional multiphase flow using level contour reconstruction method for front tracking without connectivity, J. Comput. Phys. 180 (2002) 427–470.
[24] J.S. Bai, P. Li, L.Y. Zou, T.A. Wand, Quadtree adaptive level set method for capturing interfacial instability on cartesian grid, Eng. Appl. Comput. Fluid Mech. 1 (4) (2007) 263–272.